EUROPEAN ORGANIZATION FOR NUCLEAR RESEARCH

A SEARCH FOR FRACTIONALLY CHARGED PARTICLES AT THE CERN PROTON SYNCHROTRON

J.V. Allaby, G. Bianchini°, A.N. Diddens, R.W. Dobinson†, R.W. Hartung††, E. Gygi, A. Klovning, D.H. Miller†††, E.J. Sacharidis*, K. Schlüpmann, F. Schneider, C.A. Ståhlbrandt, and A.M. Wetherell.

CERN, Geneva, Switzerland.

ABSTRACT

A search has been made for particles of fractional electric charge, produced at small angles from an internal Be target in the CERN Proton Synchrotron. No such particles were found, leading to the following upper limits for the production cross sections (90% confidence level) at 27 GeV/c incident proton momentum

Electric Charge				
$-\frac{1}{3}e$;	$\frac{d^2\sigma}{d\Omega dp} \leq 7.2 \times 10^{-39}$	at $\Theta = 0$	mrad
$-\frac{2}{3}e$;	$\leq 5.2 \times 10^{-38}$	6.5	mrad
$+\frac{1}{3}e$;	$\leq 2.6 \times 10^{-35}$	44	mrad
$+\frac{2}{3}e$;	$\leq 1.3 \times 10^{-35}$	44	mrad .

The cross section is expressed in units of $cm^2/sr.GeV/c$ per nucleon in the laboratory system and Θ is the production angle in the laboratory system.

Submitted to Nuovo Cimento
June 1969

° Present address: Dept. of Cybernetics, Academy of Sciences, Havana, Cuba.

† SRC Fellow.

†† Supported in part by the American-Swiss Foundation for Scientific Exchange.

††† Permanent address: Lawrence Radiation Lab., Berkeley, USA.

* Present address : RHEL, Chilton, Didcot, Berks., England.

1. INTRODUCTION

The remarkable successes of SU(3) symmetry in both the strong and weak interactions have led to several conjectures[1-3] that the known strongly interacting particles might consist of bound states of fundamental triplets. In particular, Gell-Mann[1] and Zweig[2] pointed out that the existence of three particles of fractional charge and fractional baryon number, usually called quarks, together with their antiparticles, would form a natural basis for SU(3) symmetry. The quantum numbers of the three quarks, p_o, n_o and λ_o, are given in Table 1. The proton would be built up from the combination (p_o, p_o, n_o) and the neutron from (p_o, n_o, n_o). During the past years, there have been many searches[4] for these particles, in the primary cosmic ray flux, in secondary particle beams from accelerators, and as stable constituents of terrestrial matter. None of these experiments have given a positive result leading to upper limits on the production cross section for quarks, which appear quite stringent until examined in the light of some theoretical model.

The most economical way to produce quarks in nucleon-nucleon collisions is by pair production

$$N + N \rightarrow N + N + Q + \bar{Q} \qquad (1)$$

or by dissociation

$$N + N \rightarrow N + Q + Q + Q \qquad (2)$$

In the absence of any detailed theory for the dissociation process (2), it is instructive to compare the experimental limits on quark production with those estimated from statistical model calculations[5] for quark pair production, reaction (1). When normalized to known antiproton cross sections and assuming isotropic production in the centre-of-mass system, predicted rates are in fact of the same order of magnitude as the available upper limits from accelerator experiments for quark masses up to about 3 GeV.

The purpose of the present experiment, which used a 26-27 GeV internal proton beam at the CERN proton synchrotron, was to improve the sensitivity of accelerator experiments by several orders of magnitude. The experiment was conceived to detect fractionally charged particles with the minimum restriction on the other properties of these particles, however the final design has the following limitations:

1. The available machine energy implies an upper limit to the quark mass accessible. At 27 GeV/c incident proton momentum the energy available in the proton-proton centre-of-mass system is 7.24 GeV. Thus quarks of mass up to about 2.7 GeV can be produced in the pair production reaction (1), while in the dissociation reaction (2) the average quark mass cannot exceed about 2.1 GeV. Quarks with these maximum masses would have laboratory momenta of about 10 and 7.8 GeV/c respectively.

2. The detection system extended to about 90 m from the target; thus the present experiment would not detect efficiently quarks of lifetime much less than 10^{-8} sec. However, Gell-Mann[1] has pointed out that, if quarks exist, at least one fractionally charged particle must be stable as a result of charge and baryon number conservation.

3. About 25 gm/cm^2 of detecting material was needed in the beam channel to provide a reliable charge measurement. If quarks have an anomalously high interaction cross section, the sensitivity of the experiment would be correspondingly reduced.

On general grounds it is likely that quark production would show the strong damping at high transverse momenta characteristic of high energy strong interaction. This damping would reduce the sensitivity of previous searches, using secondary beams with transverse momenta from .5 to 1.0 GeV/c by an order of magnitude. In the present experiment much emphasis was put on detecting quarks produced near to the forward direction.

The ionization of a charged particle is proportional to the square of its electric charge, and therefore fractionally charged quarks can be recognized by an anomalous ionization. In this experiment scintillation counters placed along the beam channel measured the ionization of the particles. As it is believed that the response of scintillation phosphors is linear in ionization even for levels as low as one tenth of minimum ionization, it is relatively easy to make a sensitive detection system using rather simple equipment. The experiment was sensitive to particles of ionization between 0.1 and 0.85 that of fast pions. The information from the scintillation counters was supplemented, part of the time, by an isotropic spark chamber[6], operated in the avalanche mode, with which the particle ionization could be measured also.

2. A SEARCH FOR NEGATIVE QUARKS USING A SUPERMOMENTUM BEAM CHANNEL

2.1 The beam channel

A quark of charge q in units of the electronic charge e and momentum p will behave in a magnetic beam channel as if it were a particle of integral charge and momentum p/q since the deflection of charged particles by magnetic fields is proportional to q/p. With this in mind, a secondary beam channel was laid out at 0 mrad production angle from an internal target to accept negative integrally charged particles having a momentum $\simeq$ 1.2 times the primary proton momentum. The particle momentum transmitted by the channel was linked to the primary proton momentum, since the first beam transport element was the 4 m long synchrotron magnet downstream from the target. With the accelerator running at 27.2 GeV/c, the beam momentum was set to 32.6 GeV/c, thus accepting quarks with $q = -1/3$ and of momentum 10.9 GeV/c. This momentum is near to the maximum of the four-body phase space for the reactions (1) and (2). Since energy-momentum conservation forbids the production of integrally charged particles with 32.6 GeV/c in collisions of a single proton on a stationary target, the beam channel acts as a "supermomentum" filter, sufficient bending being provided to prevent the transmission of integrally charged particles along legal trajectories.

The beam channel would also transport quarks of charge $q = -^2/_3$ and of momentum 21.7 GeV/c; however, this did not correspond to a favourable region of phase space and a search for such particles was made at lower momenta (see section 3).

The beam layout is shown in Fig. 1, and consisted of a double-focusing spectrometer having a dispersive focus F_1 inside the field lens Q_6 and a dispersion compensated focus at F_2. The beam was parallel in the dipole magnets M_1, M_2 and M_3, M_4 each pair giving a bending of 60 mrad. The solid-angle acceptance of the beam was $\Delta\Omega = 80\,\mu sr$ with a momentum bite $\Delta p/p = 13\%$. The beam left the synchrotron vacuum chamber through a thin window, and was transported in vacuo up to the field lens Q_6.

In order to be able to tune the beam with pions, an auxiliary magnet M_0 could be positioned by remote control on the beam axis to bend negative particles in the 20 - 28 GeV/c momentum range with a production angle of a few milliradians, down the beam line. The trajectories of such particles deviated by only about 1 cm from the computed quark trajectory in the synchrotron magnet, so the test particles passed through about the same magnetic field as would quarks. The properties of the beam were studied in the momentum range 20 - 28 GeV/c using two small scanning counters placed at the foci F_1 and F_2. The beam was found to behave in accordance with calculations in this momentum range, which gave full confidence that it would also do so when operated in the supermomentum mode. The calibration curves of all dipole magnets were checked using floating wire techniques to allow safe extrapolation from 26 GeV/c to 32.6 GeV/c.

Two counter telescopes monitored charged particle fluxes proportional to the interactions of protons in the target. They are shown in Fig. 1 as A_{12}, which viewed the internal target at a large angle, and M_{123}, which was sensitive to forward-produced particles selected by the magnetic field of the synchrotron and the magnet M_0.

2.2 The detection system

The detection system was confined to the region outside the accelerator shielding and comprised the following:

i) Six trigger counters, T_1 to T_6, each made of 1 cm thick plastic scintillator having transverse dimensions larger than the beam at the corresponding position. These counters formed a sixfold coincidence, T_{123456}, with a resolving time of ±50 nsec, large enough to detect both highly relativistic and heavy slow particles passing down the beam channel. The photomultiplier gain was such that the coincidence efficiency was $\geq 99\%$ for light pulses of 0.08 times the intensity of the scintillation light produced by fast pions.

ii) Six pulse-height measuring counters, PH_1 to PH_6, placed adjacent to the T counters, being 2 cm thick in the case of PH_1 to PH_4 and 5 cm thick for PH_5 and PH_6. Their transverse dimensions were slightly larger than those of the corresponding trigger counter in order to avoid possible small pulses due to edge effects. Tests with a light source and masks showed that the response of all pulse-height counters was a linear function of light input over at least the range 1 to 1/10 minimum ionizing. Their resolution (full width at half height) was about 25% for minimum ionizing particles.

iii) A 10× 10× 11 cm^3 isotropic spark chamber[6]) placed at the achromatic focus F_2. This was filled with a 70% Ne-30% He mixture (Henogal) at a gas pressure of one atmosphere. The chamber was rendered sensitive by a triangular pulse of 250 kV peak amplitude, with a full width at half height of 5 nsec, applied ~350 nsec after the passage of the triggering particle. Photographs of the chamber were taken in a direction perpendicular to the electric field. Because of the weakness of the light signals coming from the chamber, amplification using an image intensifier was necessary. In this mode of operation, the avalanche amplification was sufficiently small to enable a measurement of the primary ionization of a

particle to be made[7,8]. For a charge one minimum ionizing particle passing through the chamber, the observed number of avalanches was ~50 (Fig. 2).

iv) Two 3 m long threshold Čerenkov counters, C_1 and C_2, the former filled with hydrogen gas at 10 kg/cm^2 and sensitive to particles with a $\beta \geq 0.998$, and the latter filled with ethylene gas at 10 kg/cm^2 and sensitive to particles with a $\beta \geq 0.993$.

v) A time-of-flight measurement between T_1 and a double coincidence T_{56}. The time resolution was ± 0.5 nsec, thus distinguishing particles with $\beta \leq 0.99$ from mesons and nucleons in the beam.

vi) A muon counter, μ, placed behind a 1.5 m iron block to provide information on the interaction properties of the triggering particle.

Because of the filtering characteristics of the beam layout, the trigger rate from the coincidence T_{123456} was sufficiently low to enable this alone to be taken as a possible quark signature. Such a trigger initiated the following data-recording sequence:

a) The dynode signals from the pulse-height counters, PH_1 to PH_6, were displayed on an oscilloscope and photographed.

b) The anode signals from counters PH_1 to PH_6, C_1, C_2 and μ were passed through linear gates, opened by the event trigger T_{123456}, and their areas digitized and recorded on scalers.

c) Time-of-flight data between T_1 and T_{56} was similarly digitized.

d) Both the output of the image intensifier viewing the spark chamber, and the oscillogram of the high voltage pulse applied to the chamber were photographed.

The scaler data from (b) and (c) together with relevant monitor data were recorded on punched cards, after each event trigger, for subsequent analysis.

Figure 3 shows a logic diagram of the electronics used in the triggering and pulse-height recording systems.

2.3 Data-taking and checking procedures

All trigger and pulse-height counters were provided with solid state light pulsers so that the sensitivity to fractionally charged particles could be periodically checked. Quark-like events could be easily simulated by a suitable adjustment of the light pulser drive-current. The light-pulser system was used to check the photomultiplier sensitivity and the stability of the associated electronics at least once every 12 hours. Every eight hours, negative pions were sent down the beam channel, using magnet M_0, in order to check the operation of the spark chamber.

The accelerator operated with a cycling time of 2.5 sec during the experiment, and accelerated $\sim 9 \times 10^{11}$ protons per pulse of which about 70% were made available for the target used in this experiment. Data were taken during approximately 2.5×10^5 pulses, and a total of 3400 events were recorded during this time.

2.4 Data analysis

Three independent searches were made for possible quark candidates by inspection of i) the digitized pulse-heights and time-of-flight data on punched cards, ii) the oscilloscope display photographs of the pulse-height counter dynode signals and iii) the streamer chamber photographs. Fig. 4 shows a comparison of the oscilloscope displays for a typical trigger and a simulated quark event, and Fig. 5 the pulse-area and time-of-flight spectra for event triggers and pions. It was found that even a minimal requirement "pulses in PH_1 to PH_4 with heights ≤ 0.85 times minimum ionizing" was sufficient to reject all events. However, for a conservative analysis, all events with at least three low pulse-heights in the first four PH counters were cross-checked with the spark chamber data.

It was important to recognize and exclude conditions which might simulate reduced ionization in the spark chamber. The following were the most likely possibilities.

i) A voltage pulse which had too small an amplitude or length would result in lower amplification, so that not all avalanches would be registered on film. Such events were excluded by recording for each event the high-voltage pulse shape. A second means of identifying such events was by the reduced length and intensity of the avalanches.

ii) Primary electrons may be lost before one applies the high-voltage pulse, by attachment to electro-negative gases which are released from the chamber walls. By flushing the chamber regularly (every eight hours) it was possible to keep such losses negligibly small.

iii) A few electrons might be left from an old track, suggesting a sub-normally ionizing particle passed through. Diffusion, however, gives such tracks a very characteristic appearance.

iv) Primary electrons of a track that is parallel to the spark chamber wall at a distance less than 1 mm may be lost by diffusion to the wall. Such events could only have been excluded by stereo photography.

The spark chamber photographs were scanned for low ionization tracks corresponding to possible $-1/3$ and $-2/3$ quark candidates. Only one photograph showed a track with low ionization, an avalanche count of 18. However, the counter data for this event were not anomalous, and it was concluded that the most likely explanation for this event was the close proximity of the track to the chamber wall, as mentioned in point (iv) above. Thus using the complete information available no event was found that allowed a consistent interpretation as a particle of charge $-1/3$ or $-2/3$.

Under normal running conditions, it was found that counters μ and C_1 were rarely fired, suggesting that triggers were most probably due to fast, strongly interacting particles, with $\beta \geq 0.993$, which were absorbed in the iron block. These particles were most likely the result of cascade processes induced by a single particle, since a large fraction of the triggers were found to come from particles entering the beam line by some skew trajectory. This

conclusion was supported by a) the sharp decrease in singles counting rates along the beam, T_1 counting 15,000 per pulse and T_6 only 750; b) the increasing frequency of misses and saturated pulses in the PH counters going from PH_1 to PH_6 ; c) the large number of heavily ionizing and multiple prong events seen in the spark chamber.

2.5 Results

Upper limits on the quark production cross sections were derived in the following way. During a small fraction of the running time (12 hours), an aluminium target was used and the ^{22}Na activity produced in the target was measured. Since the cross section for ^{22}Na production, $\sigma(^{22}Na)$, is known to be $\simeq 10.1$ mb [9], the monitors may be absolutely calibrated. The double differential production cross section on aluminium for quarks of charge q is given by

$$\frac{d^2\sigma}{d\Omega dp}(Al) = \frac{n_q(Al)\ \sigma(^{22}Na)}{(\Delta\Omega\Delta p)_q\, n(^{22}Na)} \qquad (3)$$

where $n_q(Al)$ is the number of quarks observed from the aluminium target, $n(^{22}Na)$ is the number of ^{22}Na atoms produced during this time, and $(\Delta\Omega\Delta p)_q$ is the beam channel acceptance for quarks of charge q . Inserting $n_q(Al) \leq 2.3$ into Eq. (1), a production cross section limit per aluminium nucleus was obtained with 90% confidence.

During the main part of the data collecting runs, a beryllium target was used and the double differential quark production cross section was derived using the relation

$$\frac{d^2\sigma}{d\Omega dp}(Be) = \frac{d^2\sigma}{d\Omega dp}(Al) \cdot \frac{M(Al)}{M(Be)} \cdot \frac{n_q(Be) \cdot \Delta\sigma_M(Be)}{n_q(Al) \cdot \Delta\sigma_M(Al)} \qquad (4)$$

where $M(A)$ and $n_q(A)$ are, respectively, the number of M_{123} monitors and the number of quarks observed from target A, and $\Delta\sigma_M(A)$ is the double differential cross section for particle

production by this target into the monitor M_{123}. The ratio $\Delta\sigma_M(Be)/\Delta\sigma_M(Al)$ was taken as $A_{Be}^{2/3}/A_{Al}^{2/3} = 0.48$ since the geometrical $A^{2/3}$ law has been found to hold quite well in the high-energy region[10]. The limits on quark production per beryllium nucleus were obtained by substituting this ratio together with the known aluminium production cross section, and $n_q(Al) = n_q(Be) = 2.3$ into Eq. (4).

Table 2 shows a summary of the limits obtained for the production of $q = -1/3$ and $q = -2/3$ quarks; these are expressed per nucleus with 90% confidence. No correction has been applied for absorption or decay of quarks along the beam line. The maximum obtainable quark mass in the process (1) is also given.

3. A FURTHER SEARCH FOR QUARKS OF $q = -2/3$

A more significant search for $q = -2/3$ quarks was made by lowering the beam momentum to 22 GeV/c. This corresponded to a more favourable region of phase space, the maximum quark mass now detectable by the system in process (1) being 2.41 GeV. The beam was modified by the introduction of magnet M_0 which guided negative particles produced by incident protons of 26.4 GeV/c at 6.5 mrad down the channel.

In order to render the triggering requirement insensitive to the large flux of integrally charged particles (mostly pions) that entered the beam channel, the trigger system (Fig. 3) was modified to incorporate a pulse-height selection window. Each T counter signal was split and fed in parallel to two separate discriminators through adjustable attenuators. These were set so that the first discriminator would trigger on pulse heights larger than ~ 0.05 times those of minimum ionizing pions, and the second on pulses larger than ~ 0.85 minimum ionizing. The complement output of the second discriminator was used to veto the output of the first discriminator (Fig. 6). Thus each trigger counter had a pulse-height acceptance window of 0.05 to 0.85 times minimum ionizing giving a rejection factor against pions of 6×10^{-2}.

The over-all rejection factor obtained for T_{123456}, used as the event trigger, was 8×10^{-8}. As before, each trigger initiated the recording of pulse-height and time-of-flight data. The isotropic spark chamber was removed because owing to its long sensitive time it could not operate in the high beam flux.

The pion counting rate in the beam channel was $\sim 1.2 \times 10^5$ per machine pulse; at this intensity dead-time losses were found to be $\sim 4\%$. The efficiency of detection for simulated quarks during the normal beam spill of 200 msec was checked every 12 hours; it was typically $\sim 90\%$. This was consistent with the measured dead-time and pulse-height selection losses. A total of 1.3×10^{10} negative pions were transmitted by the system from a beryllium target. As it is possible that quark production may be enhanced on heavy nuclei by coherence effects[11], a tungsten target was used for 24 hours. During this time 3.2×10^9 pions were transmitted along the beam channel, the nominal momentum of which was lowered to 20 GeV/c in order to gain particle flux.

Both the oscilloscope display and the digitized pulse-height data were scanned for possible quark events. As before, events with three of the first four pulse-height signals ≤ 0.85 times minimum ionizing were cross-checked, but no quark candidates were found. Figure 7 shows a comparison of the A_{1234} pulse-height spectra obtained for event triggers and negative pions. A_{1234} is defined as the distance from the origin of an event in a four-dimensional pulse area space. Thus

$$A_{1234} = \left(\sum_{i=1}^{4} A_i^2 \right)^{1/2} \qquad (5)$$

where A_i are the digitized pulse areas. The position of the predicted peak for quarks of $q = -2/3$, is indicated, and the lack of candidates is clearly shown.

In order to compute the double differential cross section for quark production from a given target A, the observed number of quarks may be compared with the number of secondaries counted in the beam channel during the same time. Then

$$\frac{d^2\sigma}{d\Omega dp}(A) = \frac{n_q(A)}{n_s(A)} \cdot \left(\frac{d^2\sigma}{d\Omega dp}\right)_s (A)\, \alpha_q \qquad (6)$$

$n_q(A)$ and $n_s(A)$ are the number of quarks and secondaries observed from the target A; $(d^2\sigma/d\Omega dp)_s(A)$ is the double differential cross section for the production of secondaries; α_q is the ratio of $\Delta\Omega\Delta p$ for secondaries and quarks, $\alpha_q = 1.5$ for $q = {}^2/_3$ and $\alpha = 3.0$ for $q = {}^1/_3$.

Knowing the total number of pions counted from a particular target and their production cross section[12], one obtains a limit on the quark production cross section, per nucleus, by substituting these quantities and $n_q(A) \leq 2.3$ into Eq. (6). Table 3 shows the results obtained at 90% confidence level. The quark detection efficiency was taken to be 90% which was typically that measured for simulated quarks in normal beam conditions.

4. A SEARCH FOR QUARKS WITH $q = +{}^1/_3$ AND $q = +{}^2/_3$

The method used was essentially the same as for the $q = -{}^2/_3$ search. However, as the beam channel was not designed to accept positively charged particles, the production angle for the 20 GeV/c secondaries was (from a trajectory calculation) about 44 mrad. Any quark produced would thus have had an appreciable transverse momentum. In addition, a rather indeterminate amount of accelerator vacuum-tube material would be traversed by the beam particles (20 - 30 g/cm^2).

With a secondary proton beam intensity of $\sim 5 \times 10^4$ per pulse, a total of 5.59×10^9 protons were counted from a beryllium target, and 3.77×10^8 protons were counted from an aluminium one. The measured detection efficiency for simulated $q = +^1/_3$ and $q = +^2/_3$ quarks was $\sim 80\%$.

On examining the digitized pulse-height data, it was found that many events could be considered as possible $q = +^1/_3$ quark candidates. Figure 8 shows a comparison of the A_{1234} pulse-height spectra for event triggers and protons; A_{1234} is as defined above. Evidence for quarks of $q = +^1/_3$ is apparent. However, cross-checking such candidates with the pulse-height oscilloscope display showed that all of them had to be rejected. Such events were found to be due to normal-size pulses out of time with respect to the linear gates, often also accompanied by additional pulses. These events had the characteristics of being triggered by random coincidences, their frequency of occurence being a function of the beam intensity. That the experimental situation was less clean than in the comparable search for $q = -^2/_3$ particles can be explained by the fact that in the latter a proper beam was formed of the negative pions, whereas in the present instance the large flux of protons transported by the channel did not follow trajectories for which the beam was designed.

From the oscilloscope pictures it was concluded that no valid candidates for $q = +^1/_3$ and $q = +^2/_3$ quarks were observed, and using known proton production cross section data[12] the limits on quark production shown in Table 4 were derived. An 80% detection efficiency for quarks was used.

5. DISCUSSION OF RESULTS

The results quoted in Tables 2, 3 and 4 are the measured quark production limits per nucleus in the laboratory system. In order to derive the more fundamental limits for quark production in proton-nucleon interactions the most significant values, marked with an asterisk in the previous tables, have been divided by $A^{2/3}$ and are given in Table 5.

By making assumptions about the angular distribution and momentum distribution of the quarks the total quark production cross section may be derived. The usual assumptions made are isotropic production in the centre of mass and four-body phase space for the momentum spectrum in the process (1). Using this procedure and the values given in Table 5, one obtains the values of total cross section, σ_{ISO}, shown in Fig. 9 and Table 6.

Also shown in Fig. 9 are the statistical model predictions of Hagedorn[5] for quark pair production according to reaction (1). The curve labelled "1" is for particles which are supposed to be ground states of a series of resonances, curve 2 is for particles that do not have this property. Curve 1 is normalized to the antiproton production cross section at 30 GeV/c incident proton momentum, curve 2 is normalized to the antideuteron cross section. The predictions of Maksimenko et al.[5] are rather similar to the ones shown. A noteworthy feature of the statistical model is the strong mass dependence, showing a decrease of 4 orders of magnitude for 1 GeV increase in mass.

The results of the present experiment are compared to previous ones[13,14,15,16,17,18,19] in Fig. 10. The curves show the region to which a particular experiment was sensitive. Where necessary, the curves have been calculated according to the prescription of this paper (90% confidence level, cross sections expressed per nucleon), using the model of isotropic CMS angular distribution and a four-body phase space (reaction (1)). Figure 10 also gives the statistical model predictions[5] for quark-pair production. The results of a search[20] for electromagnetically produced quarks are not shown in Fig. 10.

It may be concluded that the upper limit for the quark production cross section has been appreciably lowered in the present experiment. The fact that no quarks were detected can be interpreted in several ways: quarks might not exist as physical entities; or the conservation of some quantum number might prohibit their existence in free space; or they might be so massive as to be beyond the energies available at the present accelerators.

Although the cross sections quoted have been specifically calculated for charges $q = \pm 1/3$ and $q = \pm 2/3$, it should be remembered that this experiment was sensitive to the continuous range $0.3 \leq |q| \leq 0.9$. The experiment was not relevant to the question of the existence of polyquarks[1,21] with charges $|q| \geq 1$.

Acknowledgements

We are grateful to the Proton Synchrotron Division for the reliable operation of the accelerator at 27 GeV/c and 10^{12} protons per machine cycle. G. Cocconi made important contributions in the stage of the conception of this experiment. We want to acknowledge the help of R. Fortune in the execution of the experiment and of Miss I. Jarstorff in the measurement of target activations. Thanks are due to M. Ferrat and R. Donnet for excellent technical assistance.

Table 1

	B	q	I	I_Z	Y	S
p_o	$1/3$	$2/3$	$1/2$	$1/2$	$1/3$	0
n_o	$1/3$	$-1/3$	$1/2$	$-1/2$	$1/3$	0
λ_o	$1/3$	$-1/3$	0	0	$-2/3$	-1

Baryon number B, charge q in units of e, isospin I, its z-component I_Z, hyper charge Y and strangeness S of the quarks p_o, n_o and λ_o.

Table 2

Limits for the quark double differential production cross section per nucleus with 90% confidence at 0 mrad production angle and an incident proton momentum of 27.2 GeV/c.

Quark charge	Quark momentum [GeV/c]	Target material	Max. mass [GeV]	$d^2\sigma/d\Omega dp$ [cm^2/sr. GeV/c]
$-1/3$	10.9	Be	2.7	$\leq 3.1 \times 10^{-38}$ *
$-1/3$	10.9	Al	2.7	$\leq 1.9 \times 10^{-36}$
$-2/3$	21.7	Be	1.4	$\leq 1.6 \times 10^{-38}$
$-2/3$	21.7	Al	1.4	$\leq 9.7 \times 10^{-37}$

Table 3

Limits obtained for $-^2/_3$ quark double differential production cross sections, per nucleus, with 90% confidence, for an incident proton momentum of 26.4 GeV/c and a production angle of 6.5 mrad in the laboratory system

Target material	Quark momentum [GeV/c]	Number of pions counted	Pion production cross section [cm^2/nucleus]	Maximum quark mass [GeV]	$d^2\sigma/d\Omega dp$ [cm^2/sr.GeV/c]
Be	14.7	1.3×10^{10}	7.7×10^{-28}	2.4	$\leq 2.3 \times 10^{-37}$ *
W	13.3	3.2×10^{9}	3.7×10^{-26}	2.5	$\leq 4.4 \times 10^{-35}$

Table 4

Limits for positive quarks double differential production cross sections, per nucleus, with 90% confidence, at an incident proton momentum of 26.4 GeV/c and a production angle of 44 mrad in the laboratory system

Quark charge	Target material	Quark momentum GeV/c	Number of protons counted	Proton production cross section [cm^2/nucleus]	Maximum quark mass	$d^2\sigma/d\Omega dp\Omega$ [cm^2/sr.GeV/c]
+ 1/3	Be	6.7	5.59×10^9	7.2×10^{-26}	2.5	$\leq 1.1 \times 10^{-34}$ *
+ 1/3	Al	6.7	3.77×10^8	1.4×10^{-25}	2.5	$\leq 2.7 \times 10^{-33}$
+ 2/3	Be	13.3	5.59×10^9	7.2×10^{-26}	2.5	$\leq 5.6 \times 10^{-35}$ *
+ 2/3	Al	13.3	3.77×10^8	1.4×10^{-25}	2.5	$\leq 1.4 \times 10^{-33}$

Table 5

Limits obtained for quark double differential production cross sections, per nucleon, in the laboratory system, with 90% confidence. The maximum value of the quark mass is the one applicable for the production reaction (1) given in the text.

Quark charge	Incident proton momentum [GeV/c]	Quark momentum [GeV/c]	Quark production angle [mrad] (LAB)	Max. quark mass [GeV/c]	$d^2\sigma/d\Omega dp$ [cm^2/sr.GeV/c] (LAB)
$-1/3$	27.2	10.9	0	2.7	$\leq 7.2 \times 10^{-39}$
$-2/3$	26.4	14.7	6.5	2.4	$\leq 5.2 \times 10^{-38}$
$+1/3$	26.4	6.7	44	2.5	$\leq 2.6 \times 10^{-35}$
$+2/3$	26.4	13.3	44	2.5	$\leq 1.3 \times 10^{-35}$

Table 6

Upper limits on the total cross sections σ_{ISO} for quark production, derived from the differential cross sections of Table 5, assuming an isotropic distribution in the centre of mass, four-body phase space and reaction $p + p \rightarrow p + p + Q + \bar{Q}$. The cross sections are given for several quark masses, m_Q. They are expressed per nucleon and are at the 90% confidence level.

Quark Charge	m_Q = 0.5 GeV	m_Q = 1.0 GeV	m_Q = 1.5 GeV	m_Q = 2.0 GeV	m_Q = 2.4 GeV
	σ_{ISO}	σ_{ISO}	σ_{ISO}	σ_{ISO}	σ_{ISO}
$-\frac{1}{3}$	2.0×10^{-38}	1.4×10^{-38}	7.8×10^{-39}	3.2×10^{-39}	4.5×10^{-40}
$-\frac{2}{3}$	1.7×10^{-37}	1.3×10^{-37}	8.5×10^{-38}	5.5×10^{-38}	1.0×10^{-36}
$+\frac{1}{3}$	8.4×10^{-35}	4.6×10^{-35}	3.6×10^{-35}	1.8×10^{-35}	3.5×10^{-35}
$+\frac{2}{3}$	4.0×10^{-35}	2.9×10^{-35}	1.9×10^{-35}	1.0×10^{-35}	1.0×10^{-35}

REFERENCES

1. M. Gell-Mann, Phys.Letters 8, 214 (1964).

2. G. Zweig, CERN TH 412 (1964).

3. F. Gürsey, T.D. Lee and M. Nauenberg, Phys.Rev. 135B, 467 (1964).

4. An extensive summary is given by
   T. Massam, CERN 68-24 (1968).

5. G. Domokos and T. Fulton, Phys.Letters 20, 546 (1966).

   M. Maksimenko, I.N. Sissakian, E.L. Feinberg and D.S. Chernavsky, Zurn.Eksp.Teor.Fiz. PISMA V REDAK., 3, 340 (1966). (English translation, JETP Lett. 3, 214 (1966)).

   R. Hagedorn, Suppl.Nuovo Cimento 6, 311 (1968).

6. E. Gygi and F. Schneider, CERN 66-14 (1966).

7. F. Schneider, CERN Internal Report AR/Int.GS/66-1 (1966).

   F. Schneider, CERN Internal Report ISR/GS/69-2 (1969).

8. F. Schneider et al., to be published.

9. J.B. Cumming, Ann.Rev.Nucl.Sci. 13, 261 (1963).

   S. Meloni and J.B. Cumming, Phys.Rev. 136, B1359 (1964).

10. T. Coor, D.A. Hill, W.F. Hornyak, L.W. Smith and G. Snow, Phys.Rev. 98, 1369 (1955).

11. B. Daugeras, R. Huson, H.J. Lubatti, J. Six, J.J. Veillet, H. Annoni, K. Moriyasu, M. Rollier, H.H. Bingham, C.W. Farwell, W.B. Fretter, Phys.Letters 27B, 332 (1968).

12. E.W. Anderson, E.J. Bleser, G.B. Collins, T. Fujii, J. Menes, F. Turkot, R.A. Carrigan, R.M. Edelstein, N.C. Hien, T.J. McMahon, and I. Nadelhaft, Phys.Rev.Letters 19, 198 (1967).

    J.V. Allaby, F. Binon, A.N. Diddens, P. Duteil, A. Klovning, R. Meunier, J.P. Peigneux, E.J. Sacharidis, K. Schlüpmann, M. Spighel, J.P. Stroot, A.M. Thorndike and A.M. Wetherell, "Particle production in proton-proton collisions at 19.2 GeV/c", paper submitted to 14th International Conference on High Energy Physics, Vienna 1968, and to be published.

13. V. Hagopian, W. Selove, R. Ehrlich, E. Leboy, R. Lanza, D. Rahm and M. Webster, Phys.Rev.Letters 13, 280 (1964).

14. W. Blum, S. Brandt, V.T. Cocconi, O. Czyzewski, J. Danysz, M. Jobes, G. Kellner, D. Miller, D.R.O. Morrison, W. Neale and J.G. Rushbrooke, Phys.Rev.Letters 13, 353a, (1964).

15. H.H. Bingham, M. Dickinson, R. Diebold, W. Kock, D.W.G. Leith, M. Nikolić, B. Ronne, R. Huson, P. Musset and J.J. Veillet, Phys.Letters 9, 201 (1964).

16. D.E. Dorfan, J. Eades, L.M. Lederman, W. Lee and C.C. Ting, Phys.Rev.Letters 14, 1003 (1965). The curve plotted has been derived by assuming an upper limit equal to the quoted upper limit for anti-triton production and by assuming production reaction (1). These authors also quote an upper limit for $q = -{}^2/_3$ particles with masses in the range 3 to 7 GeV/c (Phys.Rev.Letters 14, 999 (1965)). This value has not been plotted as such heavy quark cannot be produced according to reaction (1).

17. L.B. Leipuner, W.T. Chu, R.C. Larsen and R.K. Adair, Phys.Rev. Letters 12, 423 (1964). These authors also quote an upper limit for $q = \pm {}^2/_3$ quarks that have traversed 1.5 kg/cm^2 of iron. This value has not been plotted.

18. P. Franzini, B. Leontic, D. Rahm, N. Samios and M. Schwartz, Phys.Rev.Letters 14, 196 (1965).

19. Yu.M. Antipov, N.K. Vishnevskij, F.A. Ech, A.M. Zajtsev,I.I. Karpov, L.G. Landsberg, V.G. Lapshin, A.A. Lebedev, A.G. Morozov, Yu.D. Prokoshkin, Yu.V. Rodnov, V.A. Rybakov, V.I. Rykalin, V.A. Sen'ko, B.A. Utochkin, V.P. Chromov, IHEP Preprint CEPH 68-72 (1968) and to be published.

20. E.H. Bellamy, R. Hofstadter, W.L. Lakin, M.L. Perl and W.T. Toner, Phys.Rev. 166, 1 391 (1968).

21. J.J. de Swart, Phys.Rev.Letters 18, 618 (1967).

FIGURE CAPTIONS

Fig. 1 : Layout of the beams.

Fig. 2 : A typical isotropic spark chamber picture for a charge-one, minimum ionizing particle.

Fig. 3 : Trigger and pulse-height recording logic. The "START-RECORDING" signal initiates the recording of scaler data on punched cards and the camera operation. During this time the "BUSY" signal inhibits further event triggers.

Fig. 4 : The oscilloscope display of the pulse-height counter dynode signals for a typical event and for a simulated quark event.

Fig. 5 : The digitized pulse-height and time-of-flight spectra collected in the search for $q = -{}^{1}/_{3}$ quarks. The upper spectra are for pions of 26 GeV/c, the lower spectra are for triggers obtained during the super momentum operation. The peaks at the top-end of the pulse-height spectra are due to saturation in the shaping amplifiers and encoders. The scale on the abscissa of the time-of-flight spectrum corresponds to 1 nsec = 90 digits.

Fig. 6 : Modification to each trigger counter logic in order to reject integrally charged particles. The attenuators are set such that Discriminator 1 gives a "YES" signal for all particles ionizing more than 0.05 times minimum ionizing, whereas Discriminator 2 gives a "NO" signal for particles more than 0.85 times minimum.

Fig. 7 : The digitized pulse-height spectrum A_{1234} (defined in the text) in the search for $q = -{}^{2}/_{3}$ quarks. The upper spectrum is for pions of 26 GeV/c, the lower spectrum is for triggers obtained during the search for quarks.

Fig. 8 : The digitized pulse-height spectrum A_{1234} (defined in the text) in the search for $q = +\,{}^{1}/_{3}$ and $q = +\,{}^{2}/_{3}$ quarks. The upper spectrum is for pions of 26 GeV/c, the lower spectrum is for triggers obtained during the search for quarks. The few events at $q = +\,{}^{1}/_{3}$ are not due to quarks, as evinced by the oscilloscope pictures.

Fig. 9 : Total cross section limits calculated for an isotropic CMS angular distribution and four-body phase space in the reaction (1) for the results of the present experiment. The total cross sections are expressed per nucleon. Curves 1 and 2 are statistical model predictions.

Fig. 10: A summary of machine experiments carried out to date searching for fractionally charged particles of $q = \pm\,{}^{1}/_{3}$ and $q = \pm\,{}^{2}/_{3}$. The total cross sections are expressed per nucleon and have been calculated assuming isotropic CMS angular distribution and four-body phase space according to reaction (1). The statistical model predictions are also shown, as in Fig. 9.

Curve A : see Hagopian et al.[13]
" B : see Blum et al.[14]
" C : see Bingham et al.[15]
" D : see Dorfan et al.[16]
" E : see Leipuner et al.[17]
" F : see Franzini et al.[18]
" G : see Antipov et al.[19]
" H : this experiment.

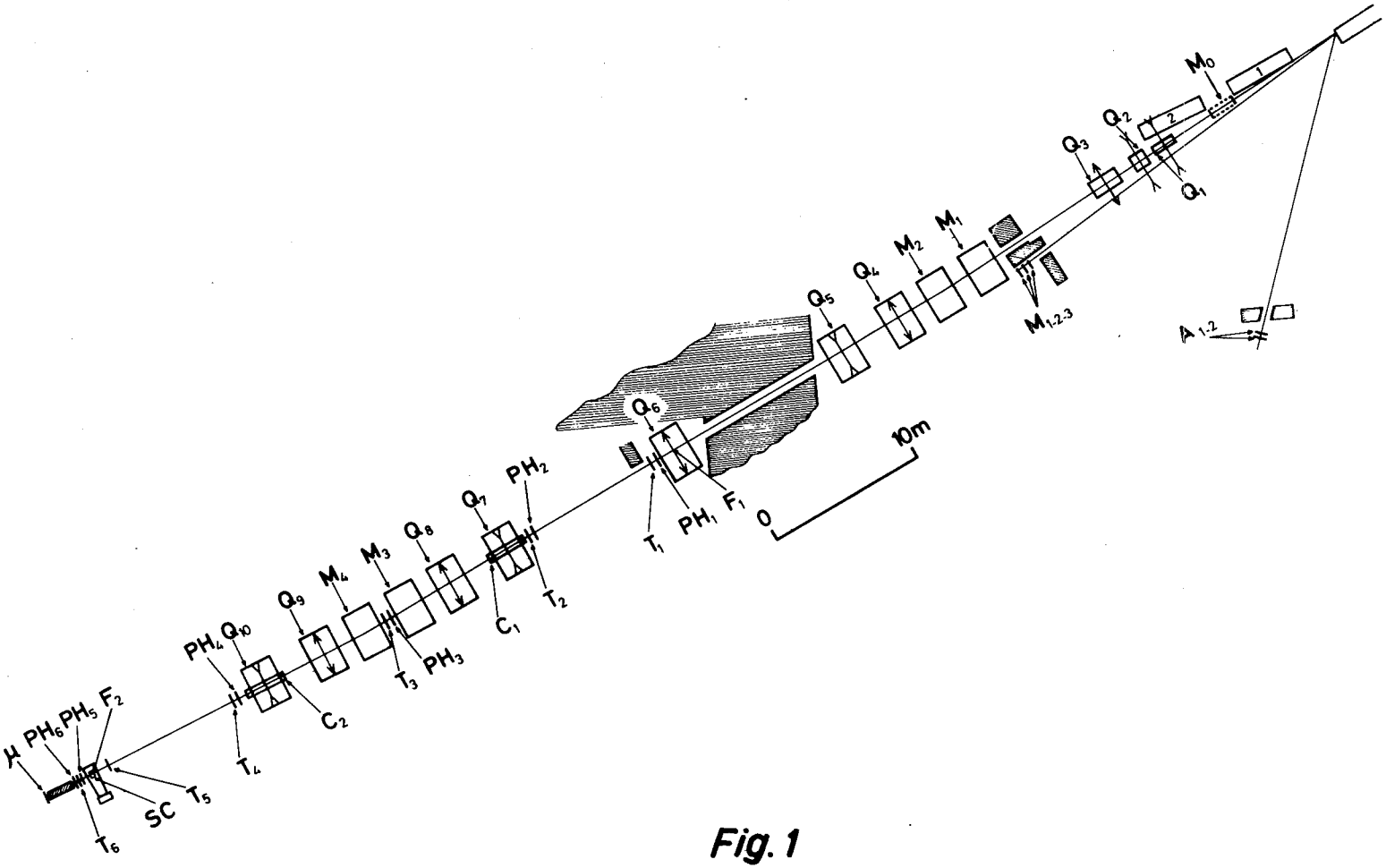
μ
PH6
PH5
F2
T6
SC
T5
T4
PH4
Q10
C2
Q9
M4
M3
Q8
T3
PH3
Q7
C1
PH2
T2
Q6
T1
PH1
F1
0
10m
Q5
Q4
M2
M1
M1,2,3
Q3
Q2
Q1
M0
A1,2

Fig. 1

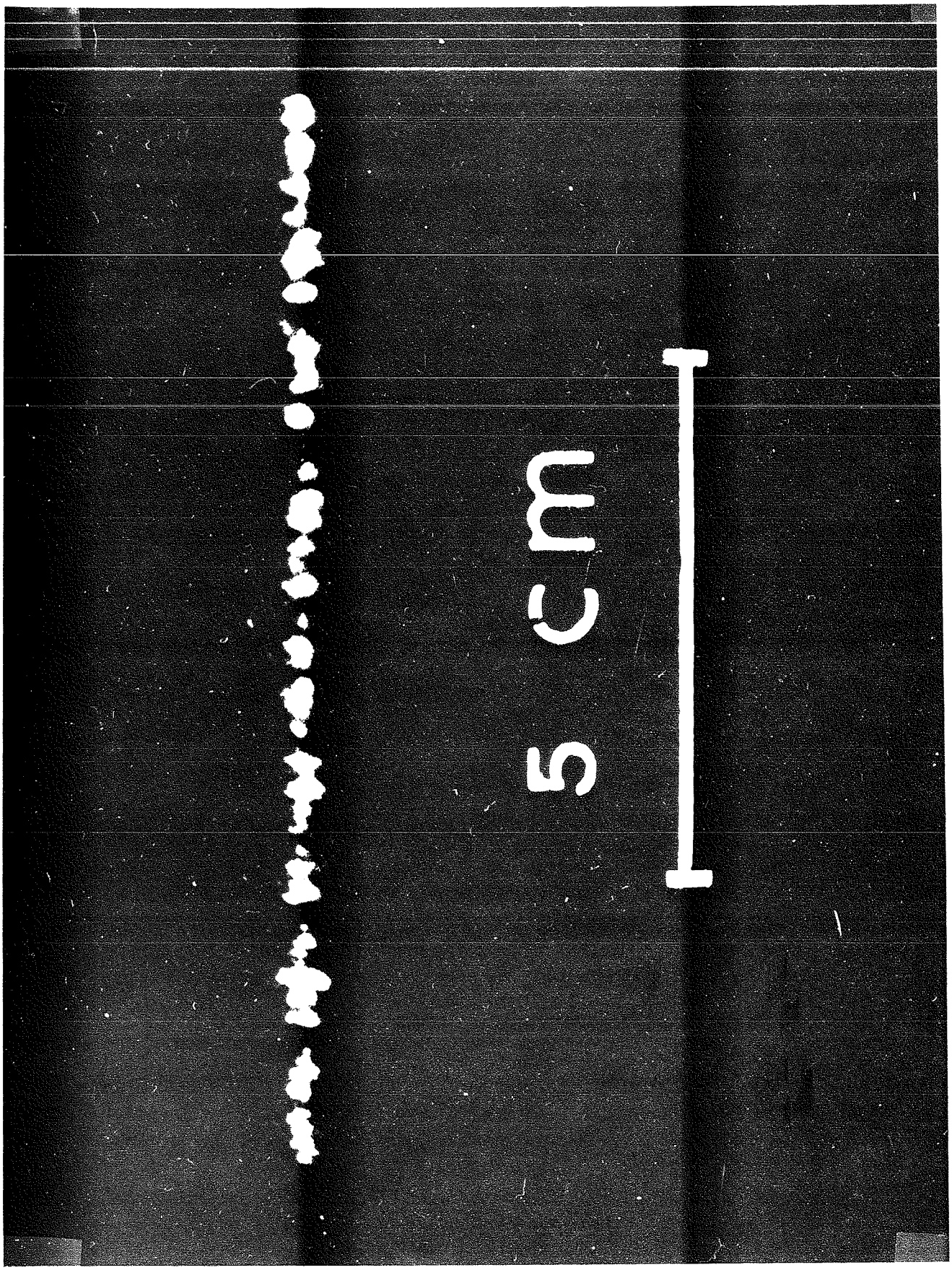

Fig. 2

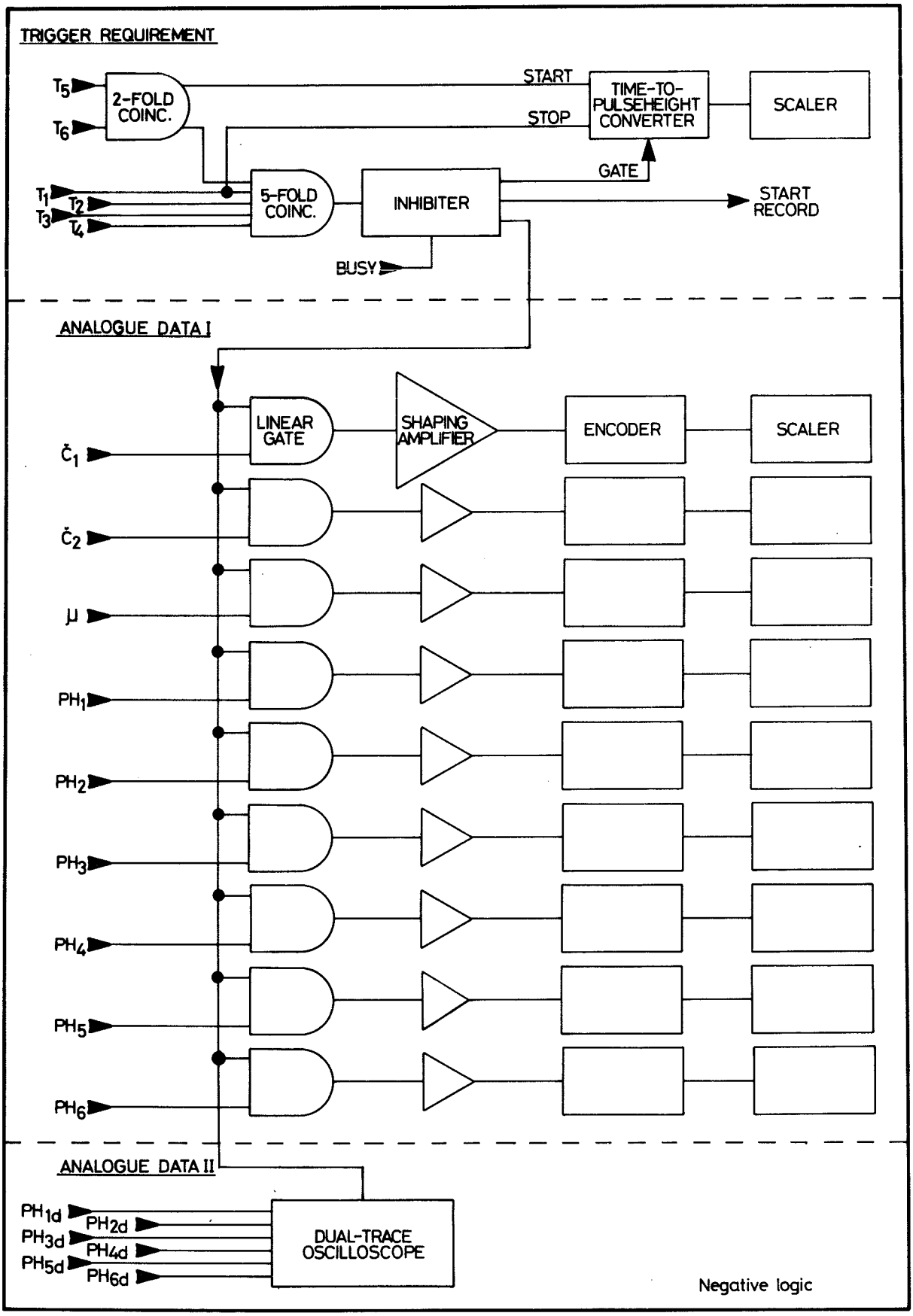
TRIGGER REQUIREMENT
T5
T6
2-FOLD COINC.
START
STOP
TIME-TO-PULSEHEIGHT CONVERTER
SCALER
GATE
T1
T2
T3
T4
5-FOLD COINC.
INHIBITER
START RECORD
BUSY
ANALOGUE DATA I
LINEAR GATE
SHAPING AMPLIFIER
ENCODER
SCALER
Č1
Č2
μ
PH1
PH2
PH3
PH4
PH5
PH6
ANALOGUE DATA II
PH1d
PH2d
PH3d
PH4d
PH5d
PH6d
DUAL-TRACE OSCILLOSCOPE
Negative logic

Fig. 3

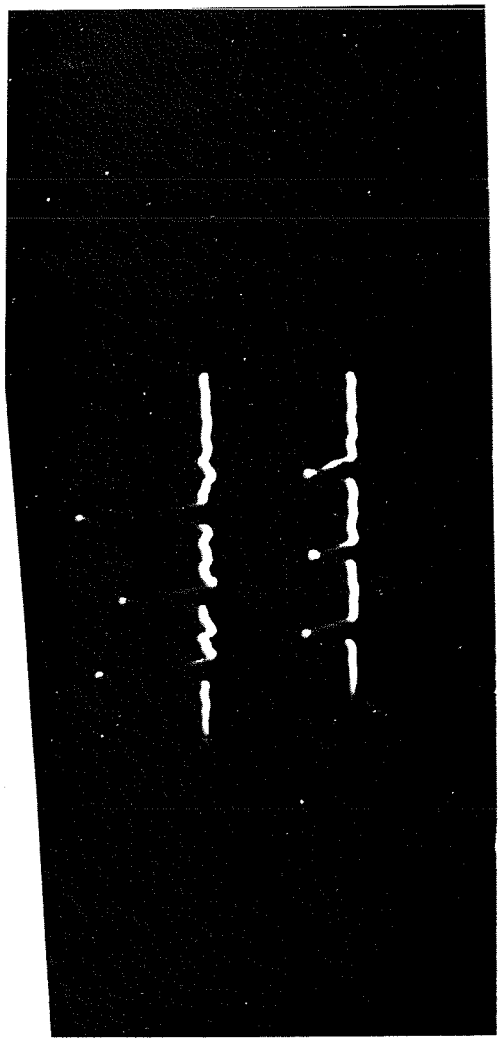

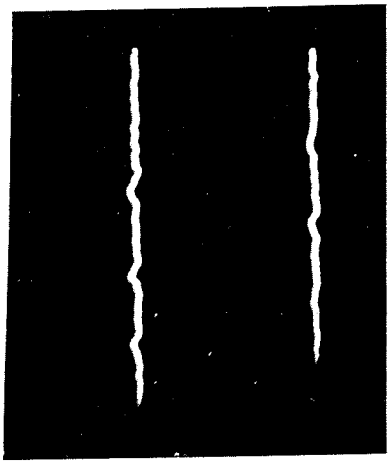

Fig. 4

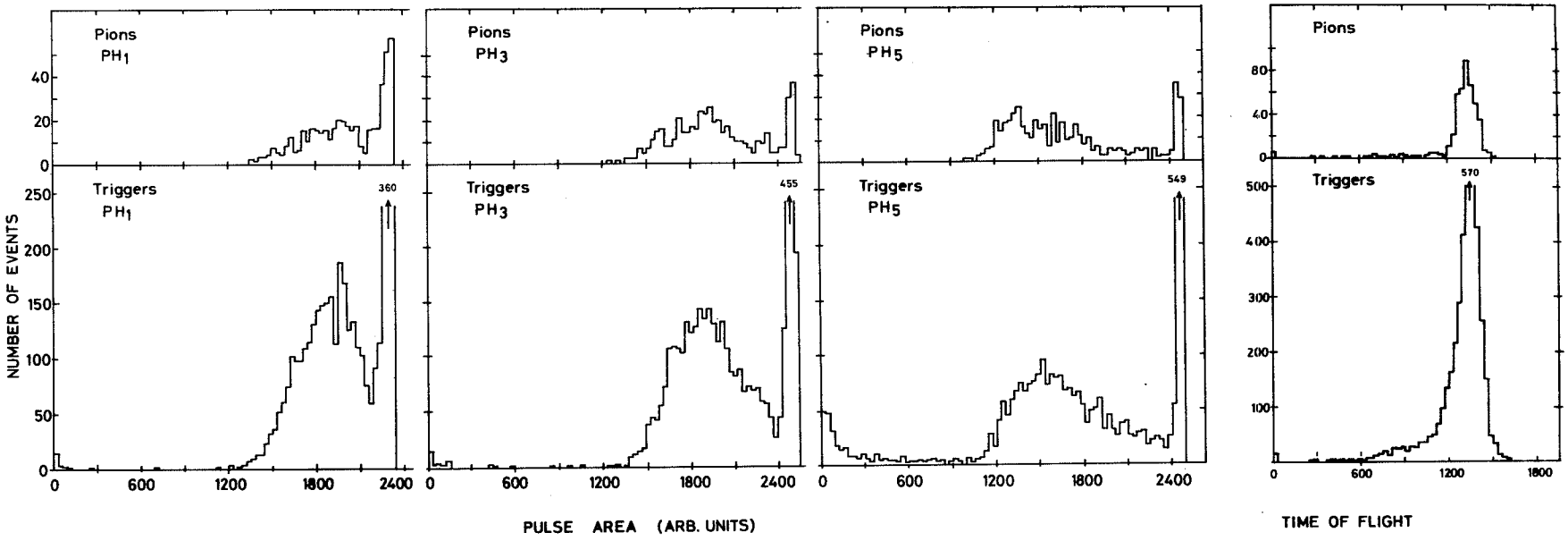
Pions
PH1
Pions
PH3
Pions
PH5
Pions
Triggers
PH1
360
Triggers
PH3
455
Triggers
PH5
549
Triggers
570
NUMBER OF EVENTS
PULSE AREA (ARB. UNITS)
TIME OF FLIGHT

Fig. 5

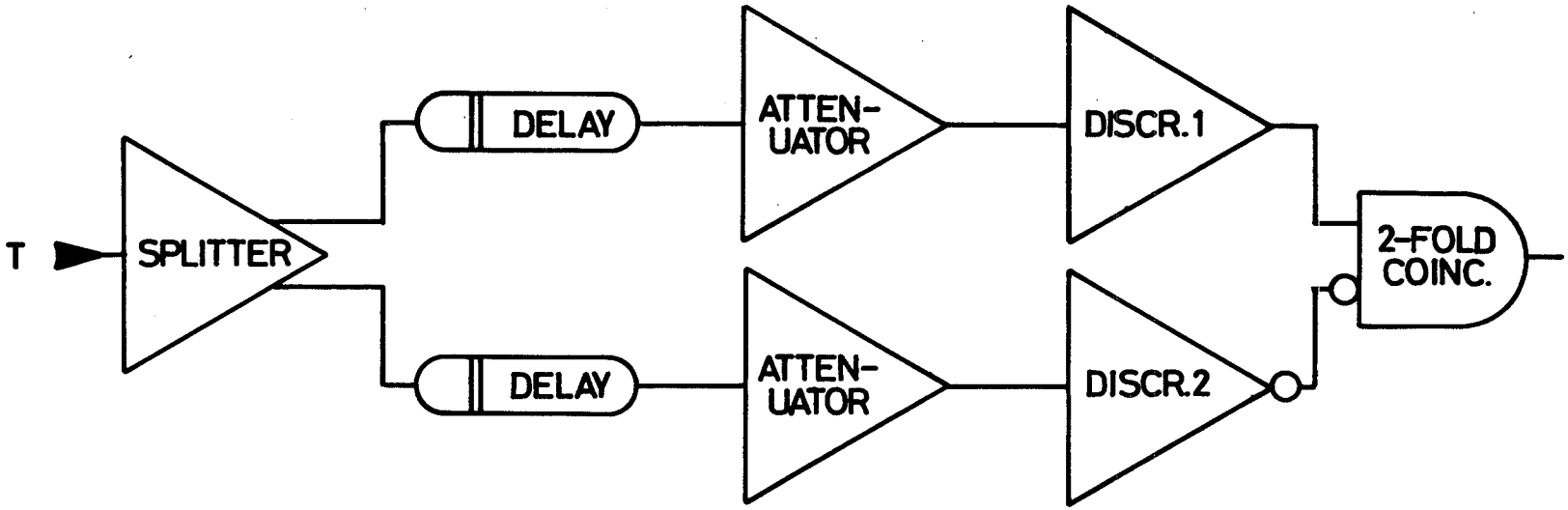
T
SPLITTER
DELAY
DELAY
ATTEN-
UATOR
ATTEN-
UATOR
DISCR.1
DISCR.2
2-FOLD
COINC.

Fig. 6

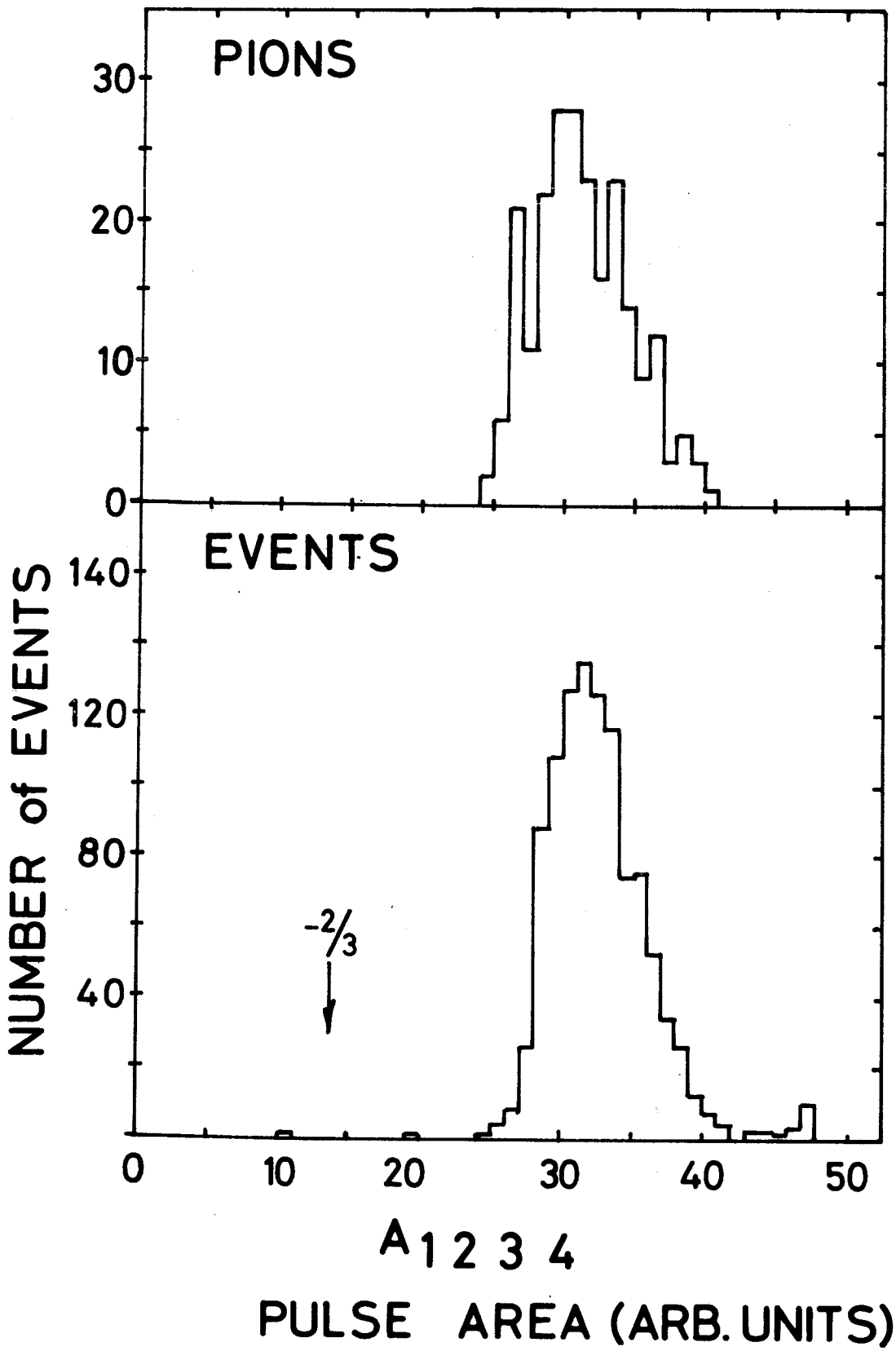
PIONS
30
20
10
0
EVENTS
140
120
80
40
-2/3
NUMBER of EVENTS
0
10
20
30
40
50
A1 2 3 4
PULSE AREA (ARB. UNITS)

Fig. 7

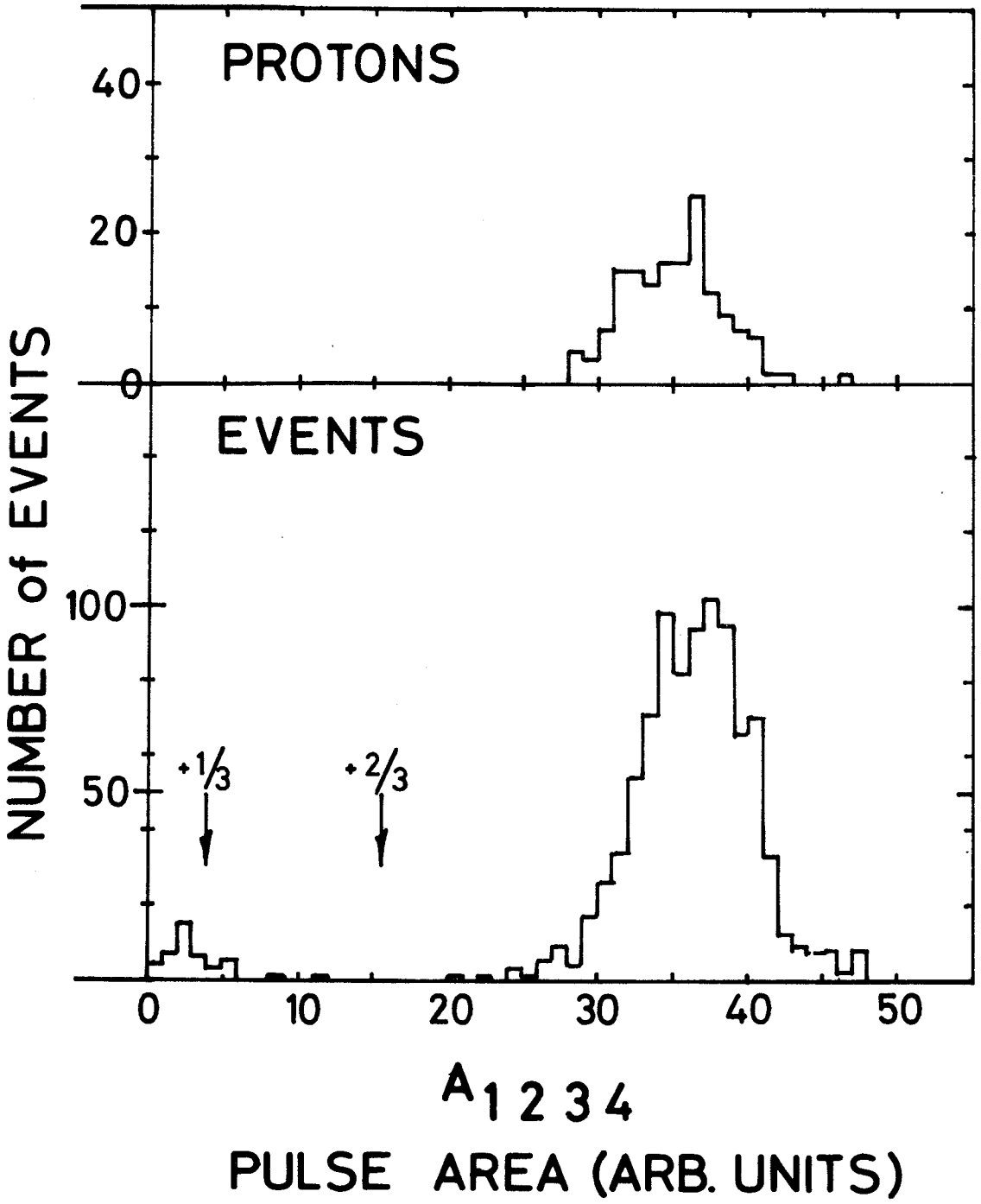
PROTONS
40
20
0
EVENTS
100
50
+1/3
+2/3
NUMBER of EVENTS
0
10
20
30
40
50
A1234
PULSE AREA (ARB. UNITS)

Fig. 8

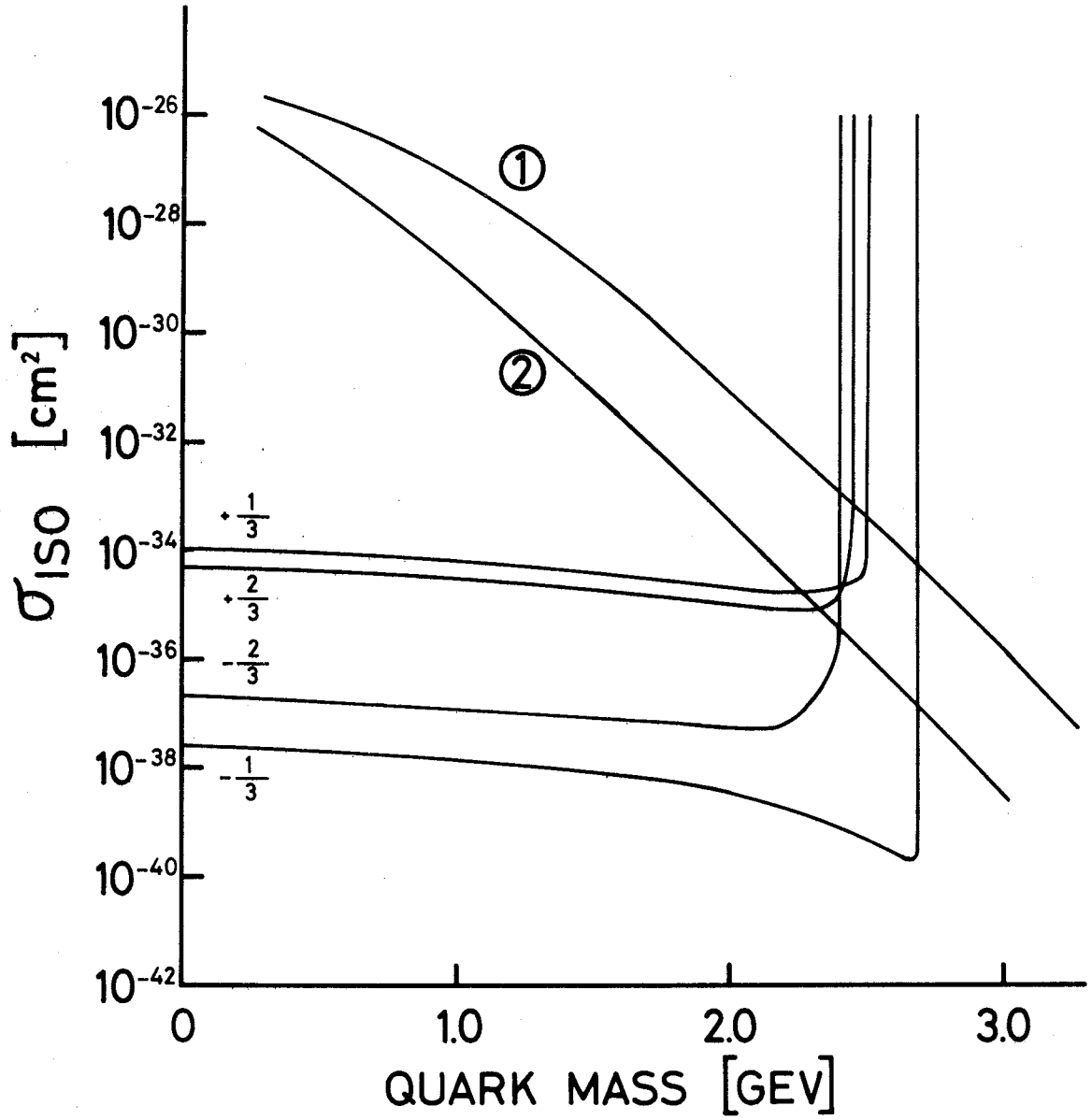
10^{-26}
10^{-28}
10^{-30}
10^{-32}
10^{-34}
10^{-36}
10^{-38}
10^{-40}
10^{-42}
σ_{ISO} [cm^2]
①
②
$+\frac{1}{3}$
$+\frac{2}{3}$
$-\frac{2}{3}$
$-\frac{1}{3}$
0
1.0
2.0
3.0
QUARK MASS [GEV]

FIG: 9

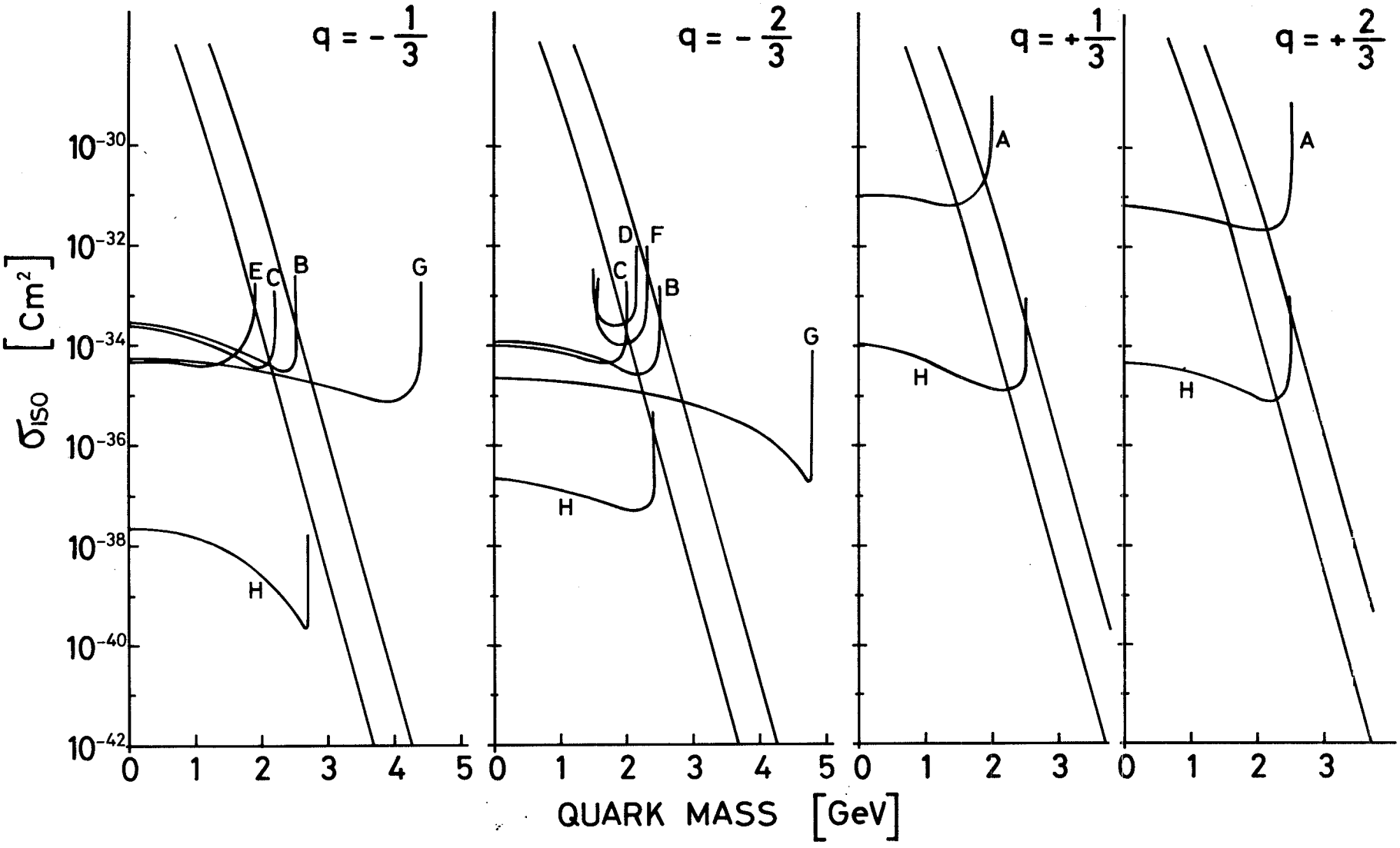
q = - 1/3
q = - 2/3
q = + 1/3
q = + 2/3
σ_{ISO} [cm²]
10⁻³⁰
10⁻³²
10⁻³⁴
10⁻³⁶
10⁻³⁸
10⁻⁴⁰
10⁻⁴²
A
B
C
D
E
F
G
H
0 1 2 3 4 5
QUARK MASS [GeV]

Fig. 10